Energy materials

Scanning probe-based nanolithography: nondestructive structures fabricated on silicon surface via distinctive anisotropic etching in HF/HNO$_3$ mixtures

Lei Wu[1], Pei Zhang[1], Chengqiang Feng[1], Jian Gao[1], Bingjun Yu[1,*] , and Linmao Qian[1]

[1] *State Key Laboratory of Traction Power, Tribology Research Institute, Southwest Jiaotong University, Chengdu 610031, China*

ABSTRACT

HF/HNO$_3$ mixtures were typical isotropic etching systems for processing silicon (Si) surface, and still suffer from difficulties in controllably fabricating nanostructures. Here, fast and anisotropic etching approach with HF/HNO$_3$ mixtures was developed to overcome this challenge. An atomic force microscope diamond tip was used for the preparation of friction-induced hillocks, mainly consisting of amorphous Si, through reciprocating sliding of Si surfaces below critical contact pressure. The hillock acted as a mask against HF/HNO$_3$ mixtures etching, forming nanostructures through subsequent distinctive anisotropic etching. The effects of volume ratio of HF/HNO$_3$ mixtures, sliding cycle, normal load, and etching time on anisotropic etching were systematically investigated to optimize fabrication parameters. Further analysis suggested that lower average dangling bond density in scanned regions may retard the breakup of Si–H bonds and polarized Si–Si backbonds, leading to lower dissolution rates compared to original Si surface. Cross-sectional high-resolution transmission electron microscope observations revealed defect-free nanostructures fabricated by the anisotropic etching. Also, several nondestructive nanostructures with different patterns were realized on Si surfaces by programming tip scanning traces. In sum, the proposed method is promising for the fabrication of controllable nano-sized functional devices by HF/HNO$_3$ mixtures.
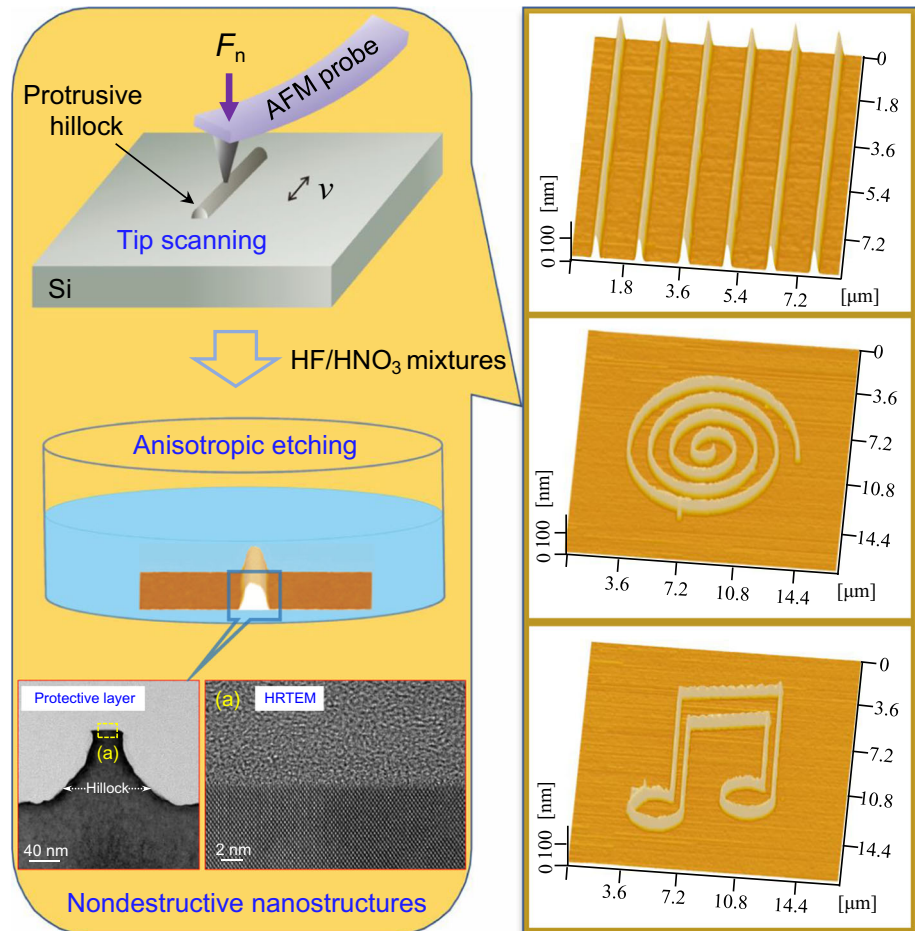
 Springer

GRAPHIC ABSTRACT

Nanofabrication of nondestructive structures on silicon surface via distinctive anisotropic etching in HF/HNO$_3$ mixtures

Introduction

With rapid development of nanoscience and nanotechnology, nanostructures have attracted increasing attention in catalysis, optoelectronics, sensing, and data storage [1–3]. Silicon (Si) is the most commonly used substrate and structural material in photovoltaics and electronic industry, and its nanostructures play a significant role in improving the performance of Si-based devices [4–7]. For instance, various surface nanostructures (e.g., nanocones, nanopyramids and nanowires) fabricated by selective removal of Si from bulk substrates can significantly improve light absorption efficiency of solar cells [8]. Patterned Si substrates were demonstrated to effectively alleviate the effect of wafer defects on epitaxial layers [9]. The use of Si nanogratings can provide better device stability for sensing [10]. Nevertheless, crystal defects induced during fabrication of Si nanostructures can degrade the optical and electrical properties of Si-based devices to some extent, strongly limiting their reliability and lifetime [11]. Specifically, defect-rich surfaces could induce rapid recombination of electron–hole pairs, thereby declining average carrier lifetime, and increase

current leakage that may amplify the noise [12]. Consequently, the development of novel fabrication approaches for nondestructive Si nanostructures is highly desirable for advanced applications [13].

Typical methods used for nanostructuring of Si substrates mainly include photolithography, ion beam lithography (IBL), electron beam lithography (EBL), and nanoimprint lithography (NL) [14–16]. However, these methods still suffer from various challenges (e.g., low resolution, high cost, and complex operating environment and the limitation of processing materials). By comparison, scanning probe lithography (SPL) is advantageous in terms of low cost, high resolution, and good flexibility. Hence, SPL is becoming an attractive approach for the fabrication of micro/nanostructures [17, 18]. Recently, combining scanning probe microscope (SPM) scratching and chemical etching, friction-induced selective etching (or so-called mechano-chemical SPL) is demonstrated to be useful for the fabrication of micro/nanostructures on Si, gallium arsenide, and quartz surfaces [19–21]. This route could address the SPL technical challenges in wear debris, tool wear, and substrate damage to some extent. During friction-induced selective etching process of Si, anisotropic etchants [e.g., potassium hydroxide (KOH) and tetramethylammonium hydroxide (TMAH)] are commonly used for the etching of scanned Si surfaces. The subsurface deformation induced by the scanning process can resist the etching, thereby forming hillock nanostructures [22]. However, the size and shape of nanostructures are restricted by crystallographic properties of Si during the etching of anisotropic etchants. Furthermore, the scanning-induced subsurface defects might impact subsequent applications of fabricated surface nanostructures. Therefore, eliminating the scanning-induced defects while keeping a flexible fabrication process of Si nanostructures is highly desirable.

A mixture of mixed hydrofluoric acid (HF) and nitric acid (HNO$_3$) is the most commonly used isotropic etching system for processing Si surfaces [23]. The mixtures are widely applied for the removal of saw-damage and obtaining low reflectivity surfaces during solar cell manufacturing [24]. Moreover, they provide flexible fabrication of micrometer-scale Si structures and present good compatibility with one-chip circuitry. This makes the fabrication of Si nanostructures without crystal defects possible. However, the etching profile of the mixtures is limited by the isotropic dissolution of Si. More

importantly, scaling down the etching dimensionality to the nanoscale is challenging, severely hindering the applications in nano-sized functional devices [25].

In this paper, low-cost and rapid approach consisting of site-controlled amorphous formation and subsequent anisotropic etching in HF/HNO$_3$ mixtures was developed to fabricate nanostructures on Si surfaces. A diamond tip was used to prepare friction-induced hillocks through reciprocating scanning Si surface. The effects of volume ratio of HF/HNO$_3$ mixtures, sliding cycle, normal load, and etching time on the formation of nanostructures were investigated in an effort to determine the optimal fabrication parameters. High-resolution transmission electron microscope (HRTEM) was utilized to view the cross section of fabricated nanostructures. The mechanism of anisotropic etching of scanned regions was clarified based on an electrochemical dissolution model. The results showed that the proposed approach was feasible for controllable fabrication of nanostructures with any layout pattern on Si surfaces.

Materials and methods

B-doped Si(100) wafers covered with a native oxide layer ($\sim$ 0.5 nm in thickness) were purchased from MEMC Electronic Materials, Inc., USA. The surface root-mean-square roughness of the wafers measured by an atomic force microscope (AFM, E-Sweep, Hitachi Instruments Inc., Japan) over an area of 2 μm $\times$ 2 μm was less than 0.1 nm. Before the fabrication, the Si wafers were ultrasonically cleaned successively in acetone and alcohol for 10 min, and then continuously rinsed with deionized water to remove surface contaminants.

An AFM diamond tip (NC-LC, Adama, Ireland) with a radius R of $\sim$ 400 nm was employed to prepare the friction-induced hillocks by reciprocating sliding under a line-scanning mode. The normal spring constant of the probe cantilever was calibrated as $\sim$ 100 N/m by MFP-3D AFM (Asylum Research, UK) using thermal noise method. Analytical grade HF [40% (w/w)] and HNO$_3$ [68% (w/w)] were purchased from Sinopharm Chemical Reagent Co., Ltd, and were used for performing etching experiments. All AFM images were scanned by contact mode using a Si$_3$N$_4$ tip (MLCT, Veeco Instruments Inc., Plainview, NY, USA) with a spring constant of 0.1 N/m.

Figure 1 Surface topographies and corresponding cross-sectional profiles of a friction-induced hillock before and after the etching in HF/HNO$_3$ mixtures for 2 s.
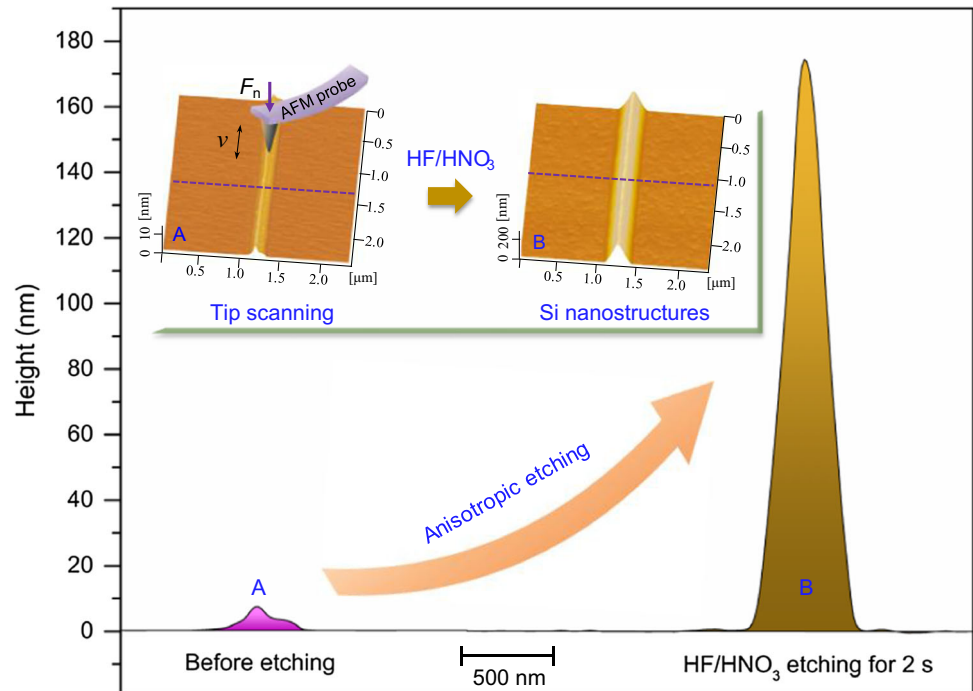
The fabrication process mainly consisted of two steps, as shown in Fig. 1. Firstly, the AFM diamond tip was used to produce protrusive hillocks instead of material removal (groove-shaped scratch) on Si surface by reciprocating sliding at an applied normal load (F_n) of 0.5–50 μN. The scanned Si samples were then immersed in HF/HNO$_3$ mixtures at the temperature of 25 ± 2 °C and relative humidity of $50 \pm 5\%$. This process significantly increased the hillock height. The microstructures of the fabricated nanostructures were observed by an HRTEM (Tecnai G2 F20, FEI, USA), and cross-sectional samples were prepared by a focused ion beam (FIB, Nanolab Helios 400S, FEI, Netherlands). To prevent the damage from FIB milling, successive deposition of an epoxy polymer and Pt layer was carried out on sample surfaces before milling process.

Results and discussion

Effects of scanning and etching parameters on anisotropic etching

Volume ratio of HF/HNO$_3$ mixtures

The volume ratio of HF/HNO$_3$ mixtures could significantly impact the etching rate of Si wafers [26]. Compared to HF-rich HF/HNO$_3$ mixtures

(HF:HNO$_3$ > 1:1, v/v), HNO$_3$-rich HF/HNO$_3$ mixtures (HF:HNO$_3$ < 1:1, v/v) presented better safety and controllability due to their relatively low etching rate. Accordingly, HNO$_3$-rich HF/HNO$_3$ mixtures should be more suitable for the fabrication of Si nanostructures [27, 28]. To investigate the concentration-dependent anisotropic etching process, various volume ratios of HNO$_3$-rich HF/HNO$_3$ mixtures (HF:HNO$_3$ = 1:200, 1:100, 1:80, 1:60, 1:40, 1:20, 1:10, 1:5, and 1:1) were used for the etching of similar friction-induced hillocks produced at F_n = 40 μN and v = 40 μm/s. After the etching of the hillocks for 2 s, the evolution of surface topography in scanned regions showed significant dependence on volume ratio, as shown in Fig. 2. At volume ratio of 1:200, no significant changes in etched topography were observed, demonstrating a ratio with poor anisotropic etching capacity. As the ratio rose from 1:100 to 1:5, the height of fabricated nanostructures dramatically increased, confirming volume ratios with excellent anisotropic etching abilities. At volume ratio of 1:1, discontinuous and irregular nanostructures were noticed, implying unsuitable ratio for Si nanofabrication. Moreover, the fabricated hillock nanostructures presented different cross-sectional profiles as the ratio increased from 1:100 to 1:5. Note that such features could hardly be realized by the etching of anisotropic etchants such as KOH solution

Figure 2 AFM topography of hillock nanostructures fabricated by $F_n = 40$ μN at 100 reciprocating cycles and post-etching for 2 s under various volume ratios. The corresponding volume ratios are marked in AFM images.
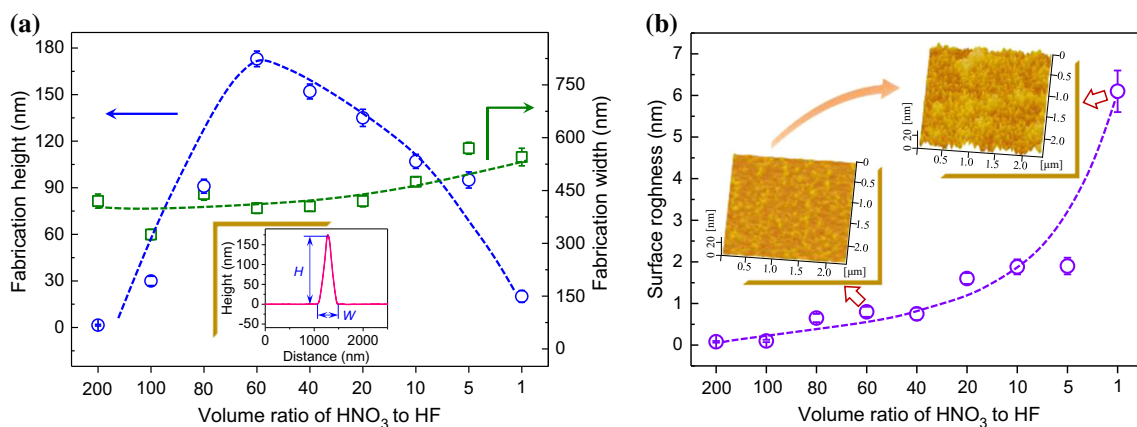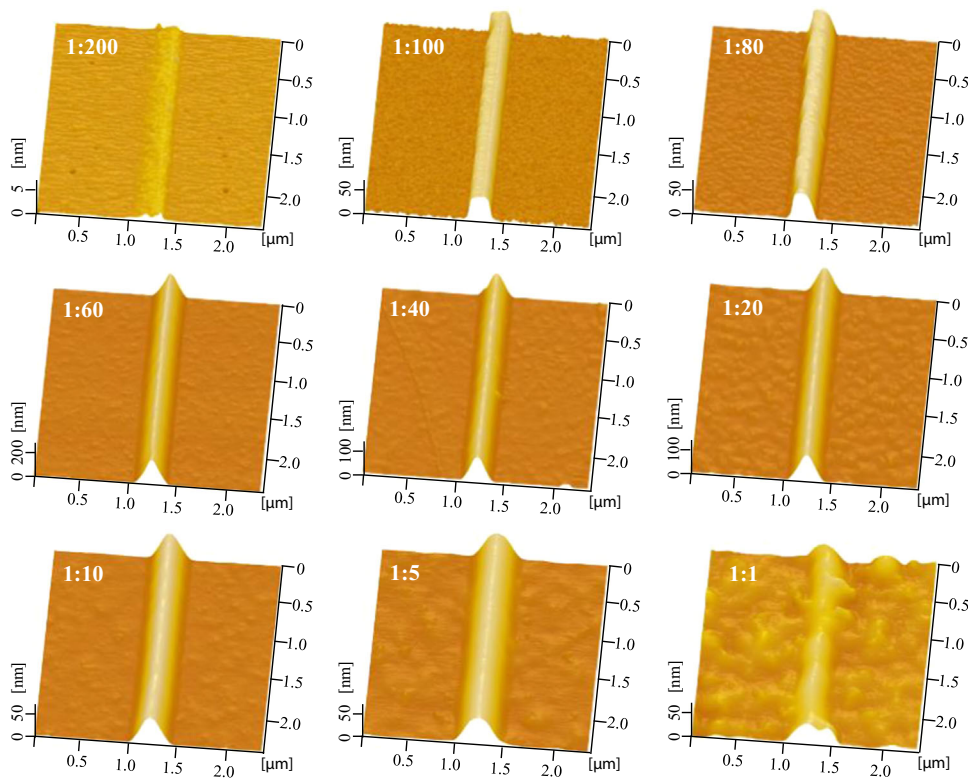
Figure 3 The effect of volume ratio of HF/HNO$_3$ mixtures on **a** the height/width of hillock nanostructures and **b** surface roughness. The dotted lines of Fig. 3a are drawn to guide the eyes for fabrication height/width, and the data are estimated from Fig. 2. The height H and width W of the hillock nanostructure are defined in the inset of Fig. 3a.

due to their intrinsic etching characteristics. The correlation between fabrication height/width and volume ratio of HF/HNO$_3$ mixtures was displayed in Fig. 3a. The fabrication height firstly enhanced from 30 to 173 nm as volume ratio increased from 1:100 to 1:60, and then gradually decreased as volume ratio further rose. Besides, the fabrication width exhibited less sensitivity to the volume ratio of HF/HNO$_3$ mixtures.

In order to understand the distinctive anisotropic etching more clearly, two Si wafers with similar friction-induced hillocks were etched by pure HF solution and pure HNO$_3$ solution, respectively. Figure S1 (In Supplementary Material) displays AFM images and corresponding cross-sectional profiles of the friction-induced hillocks before and after being etched by pure HF solution (Fig. S1a) or pure HNO$_3$ solution (Fig. S1b). It is indicated that the height of

friction-induced hillocks after being etched by pure HF solution for 2 s decreased from 3.6 to 2.7 nm, and that by pure HNO_3 solution for 2 s decreased slightly as well. Such results demonstrated that any anisotropic etching can be hardly realized by pure HF solution or pure HNO_3 solution. Therefore, the distinctive anisotropic etching in the present study can be further described as synergistic effect of HF and HNO_3 in the mixtures.

Besides, note that the performance of Si-based functional surfaces often depends on form accuracy and surface quality [29]. Therefore, it is necessary to investigate the effect of the volume ratio of HF/HNO_3 mixtures on the roughness of etched Si surfaces to provide a reference for the fabrication and packaging process of devices. To this end, the surface roughness was characterized by AFM after the etching of Si samples by different volume ratios of HF/HNO_3 mixtures for 2 s. The correlation between the surface roughness and volume ratio is presented in Fig. 3b. The surface roughness gradually increased with the volume concentration of HF solution. In particular, the surface roughness was less than 1 nm for volume ratios ranging from 1:200 to 1:40. By comparison, the surface roughness rose to $\sim$ 6.1 nm at the ratio of 1:1. The insets in Fig. 3b displayed the surface topographies etched by HF/HNO_3 mixtures at volume ratios of 1:60 and 1:1. Comprehensive consideration of anisotropic etching ability and surface roughness, volume ratios from 1:100 to 1:5 looked optimal for the fabrication of Si nanostructures. If not specified, all etching experiments were performed at ratio 1:60.

Scanning parameters

In addition to volume ratio of the HF/HNO_3 mixtures, scanning parameters may also strongly affect the formation of hillock nanostructures. To investigate the effect of sliding cycles N on fabrication height/width, several friction-induced hillocks were respectively prepared under F_n = 50 μN with N = 1, 10, 100, 200, and 400. In Fig. 4, the height of newly formed hillock nanostructures enhanced from 18 to 200 nm as N varied from 1 to 100 after the etching of friction-induced hillocks by HF/HNO_3 mixtures for 2 s. Also, the hillock height tended to stabilize at $\sim$ 200 nm for N values beyond 100. The results demonstrated that the etched hillock nanostructures were obviously affected by N, which can be

correlated with the thickness of anti-etching layer on friction-induced hillocks. In fact, the generation of friction-induced hillocks on Si surface can be dominated by mechanical interaction, which can be further described as frictional shear-induced structural deformation, such as amorphous Si (a-Si) and dislocations [30]. Correspondingly, the increase of sliding cycles N from 1 to 100 in the present study was beneficial for the formation of a-Si, resulting in the increase of the thickness of surface amorphous layer. As N further rose (beyond 100), it was expected that the thicker a-Si layer can reduce the mechanical interaction between diamond tip and bulk crystalline Si, and hence the thickness of surface amorphous layer almost trended to be stable. Consequently, the fabrication height firstly increased and then gradually trended to be stable as N increased. Certainly, the fabrication width also exhibited a similar variation trend. Therefore, it was suggested that lager N can hardly improve the barrier ability of scanned regions to resist the etching process when N reached 100. In sum, the optimal value of N for anisotropic etching of scanned regions was determined as 100 when considering the fabrication results and efficiency.

The influence of normal load F_n on the fabrication height/width was studied and the data are illustrated in Fig. 5 and S2. At F_n = 0.2 μN (corresponding to the maximum Hertzian contact pressure P_{max} of $\sim$ 1.6 GPa) [31], friction-induced hillocks can be hardly formed on Si surface. Correspondingly, no anisotropic etching phenomenon was noticed after the etching of the scanned sample by HF/HNO_3 mixtures for 2 s. This might be attributed to the absence of plastic deformation under such loading conditions. As F_n increased to 0.5 μN (corresponding to P_{max} of $\sim$ 2.1 GPa), a friction-induced hillock with a height of $\sim$ 0.55 nm was produced on Si surface. After the etching of the friction-induced hillock by HF/HNO_3 mixtures for 2 s, the hillock height reached $\sim$ 5 nm. Further increase in F_n from 0.5 to 50 μN, the height of the newly formed hillock nanostructures rose from 5 to 200 nm. Also, the hillock width enhanced from 190 to 420 nm. This may be attributed that higher normal load may induce thicker and wider deformation distributions, thereby yielding higher and wider hillock nanostructures. Consequently, normal loads from 0.5 to 50 μN can easily control the fabrication height/with.
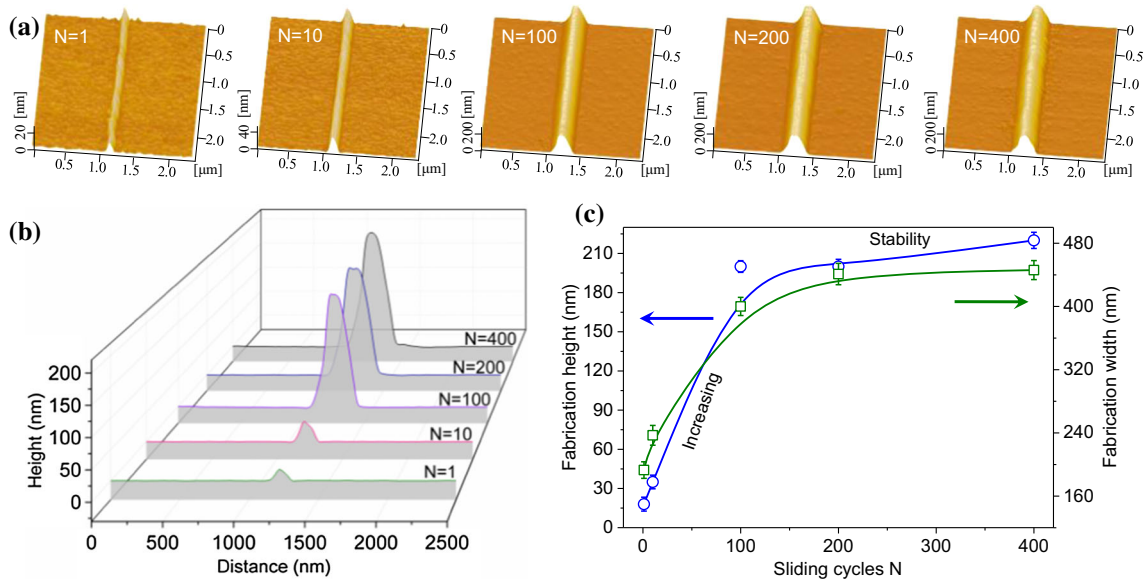
Figure 4 **a** AFM images, **b** cross-sectional profiles, and **c** fabrication height/width of produced hillock nanostructures under different sliding cycles N. The respective values of N are 1, 10, 100, 200, and 400. The applied normal load is 50 μN and etching time is 2 s.
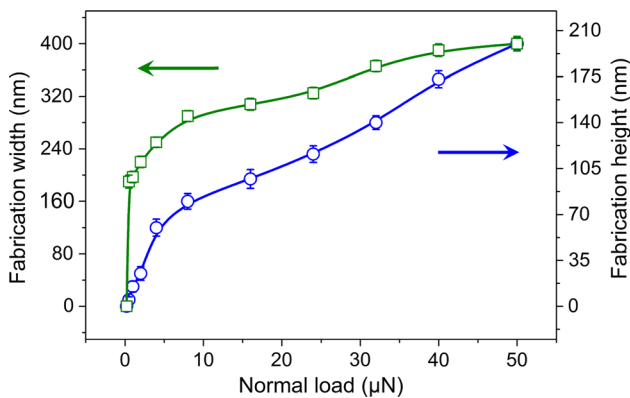
Figure 5 The change in fabrication height/width as a function of the applied normal load. The respective values of F_n are 0.2, 0.5, 1, 2, 4, 8, 16, 24, 32, 40, and 50 μN. The etching time is 2 s.
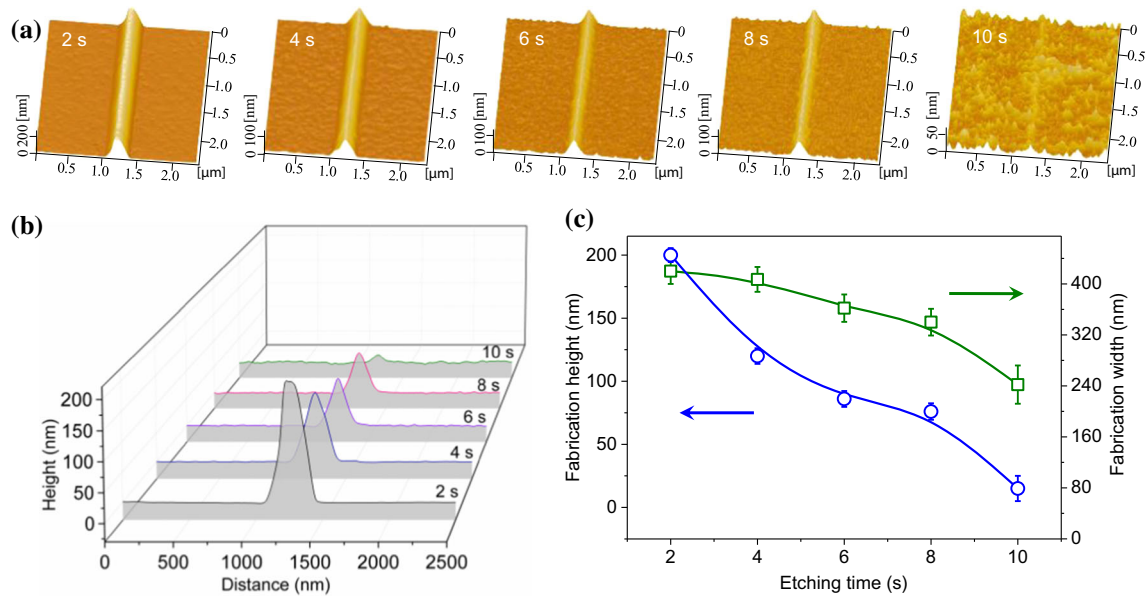
Etching time

The etching time also strongly affected the formation of fabricated nanostructures in bulk micromachining based on etching technology. In order to investigate the effect of etching time on fabrication height/width, a friction-induced hillock produced under $F_n = 50$ μN was etched by HF/HNO₃ mixtures for 2–10 s. The surface topographies of the as-obtained samples were characterized by AFM every 2 s and the results were gathered in Fig. 6. For the sample etched for 2 s, the height of fabricated hillock nanostructure swiftly rose to ∼ 200 nm. As etching time increased from 2 to 10 s, the fabrication height

gradually decreased until reaching ∼ 15 nm. The width also reduced from 420 to 242 nm. Therefore, the fabrication height/width can easily be controlled by etching time. Note that prolonged etching can result in the collapse and even final disappearance of the fabricated nanostructures. This may be attributed that the subsurface deformation in scanned regions was gradually etched away, resulting in the weakness of the anisotropic etching. In addition, the effect of etching time on surface roughness was also investigated and the data are provided in Fig. S3 of Supplementary Material. As etching time rose from 2 to 10 s, the surface roughness increased from 0.7 to 7.7 nm. Hence, short etching times (within 6 s) should be optimal for the fabrication process.

Anisotropic etching mechanism

The above results demonstrated HF/HNO₃ mixtures to possess excellent anisotropic etching nanofabrication abilities despite being typical isotropic etching systems of Si. To gain a better understanding of anisotropic etching mechanism of scanned regions, a friction-induced hillock, consisting of a-Si and deformed Si [30], was analyzed based on surface topography of scanned regions before and after being etched by HF solution and HF/HNO₃ mixtures, as shown in Fig. 7. After the etching by HF solution for 40 min, the hillock with a height of ∼ 5.5 nm evolved to form a groove with a depth of ∼ 26 nm

Figure 6 a AFM images, **b** cross-sectional profiles, and **c** fabrication height/width of produced hillock nanostructures under different etching time. The respective values of etching time are 2, 4, 6, 8, and 10 s.

Figure 7 a AFM images and **b** cross-sectional profiles of a friction-induced hillock before and after being etched by HF solution and HF/HNO$_3$ mixtures.
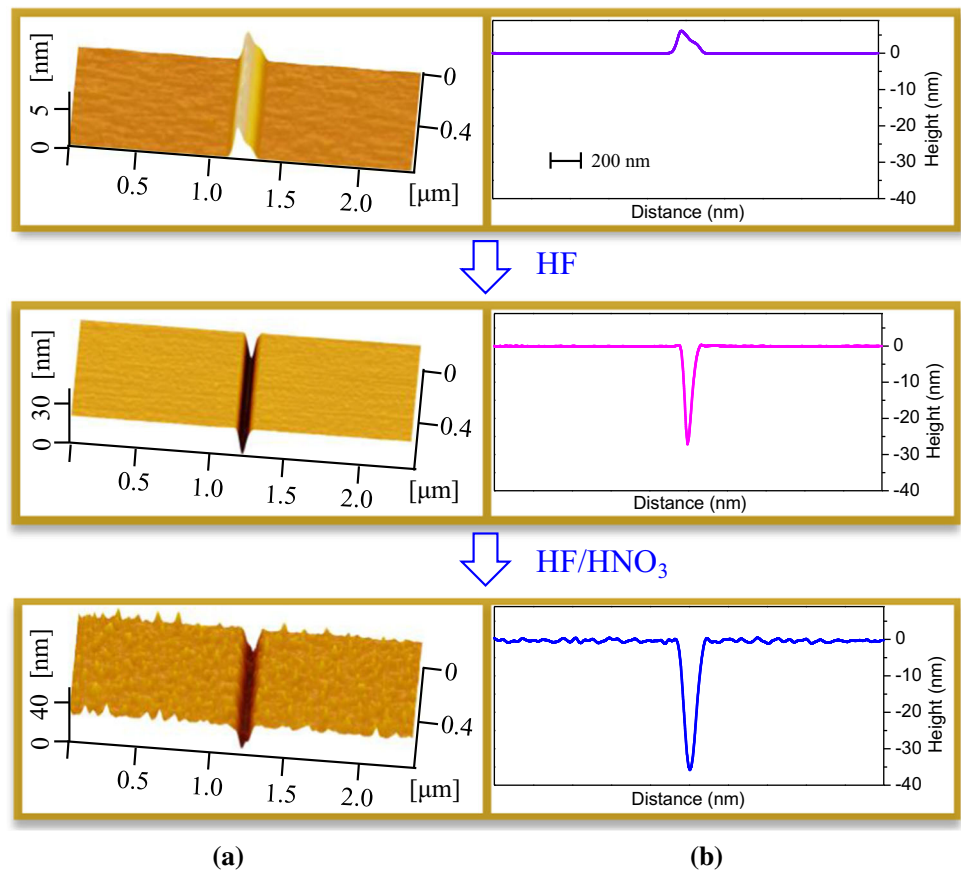
and remained to be stable with further etching. This indicated the complete removal of the topmost amorphous layer of the hillock. Further etching in

HF/HNO$_3$ mixtures for 2 s led to an increase in the groove depth to $\sim$ 34 nm (Fig. 7b). Thus, one can deduce that a-Si can resist HF/HNO$_3$ mixtures
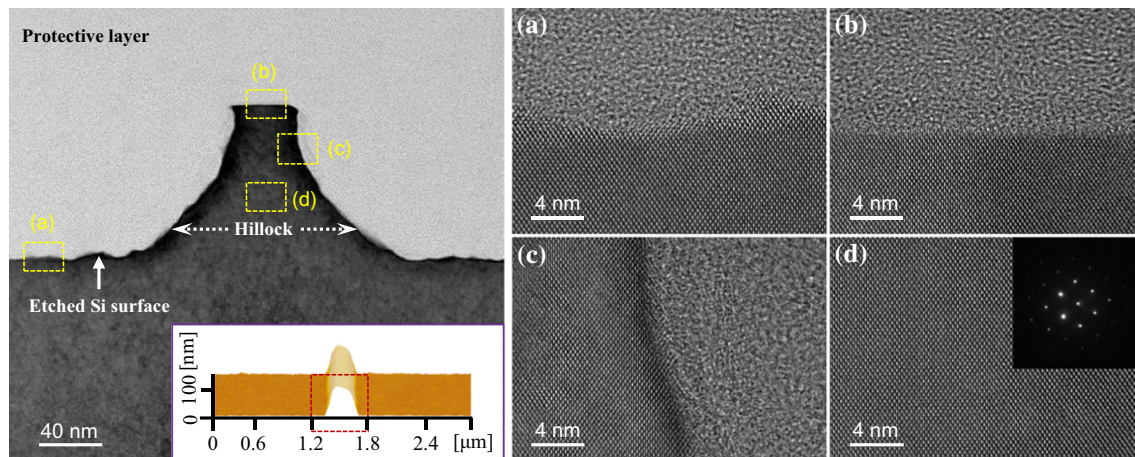
Figure 8 AFM topography and cross-sectional lattice structure of fabricated nanostructures on Si surface. The left panel shows the overall cross-section HRTEM image and AFM topography of a hillock etched by HF/HNO$_3$ mixtures for 2 s. The details of the yellow marked area are magnified in **a**–**d**.

etching, while deformed Si provided little contribution to the formation of hillock nanostructures.

To clarify the effect of scanning-induced defects on the atomic structures of fabricated hillock nanostructures, cross section of a hillock, which was produced by F_n = 32 μN and post-etching for 2 s, was prepared by FIB milling for subsequent HRTM observations. In Fig. 8, a distinct dividing line could be clearly distinguished between protective layer and the hillock. The enlarged HRTEM images showed almost perfect crystal lattice of the hillock. Moreover, a comparison of selected area electron diffraction (SAED) pattern of the fabricated hillock with that of defect-free region showed no additional diffraction spots or rings, indicating that the interior of the hillock preserved its original single-crystal structure without the presence of a-Si [32]. Note that a-Si layer can be selectively removed by HF solution [28], and hence surface topography evolution of fabricated hillock structure before and after being etched by HF solution can be used to further verify whether a-Si existed near crystal Si on the hillock structure. As shown in Fig. S4a–c, the change in the height and cross-sectional profiles of fabricated hillock structure can be hardly noticed after the etching in HF solution for 5 min, further demonstrating that the amorphous near the crystal Si on the hillock structure was protective layer rather than a-Si (Fig. 8). As a result, scanning-induced subsurface defects including a-Si and deformed Si could be gradually eliminated by the anisotropic etching, yielding nondestructive nanostructures. Besides, the HRTEM image of etched

surface from unscanned regions revealed that the etching process did not cause secondary lattice damage to Si substrates.

The etching of Si in HF/HNO$_3$ mixtures was reported as an electrochemical process [33]. During the etching, the Si surface was persistently terminated by the hydrogen groups. Oxidizing agents (i.e., HNO$_3$) could provide holes (h$^+$) for the initiation of dissolution reaction, allowing reactive species (e.g., HF or HF$_2$) to attack superficial Si–H bonds. This process allowed the replacement of Si–H bonds by Si–F bonds. Subsequently, the polarized Si–Si back bonds were attacked by the reactive species and thereby resulted in the removal of superficial Si atoms from bulk substrates. The final step involved the complexation of SiF$_4$ by HF to yield H$_2$SiF$_6$.

Based on the above results, a model was proposed to explain the anisotropic etching of friction-induced hillocks. As shown in Fig. 9a, b (Not drawn to scale), the scanning of Si surface by the AFM diamond tip transformed the monocrystalline structure of Si atoms in scanned regions into a-Si or deformed Si. Since the atomic arrangement of a-Si became out of order, the average dangling bond density in scanned regions was lower than in the original Si surface [34]. During the etching in HF/HNO$_3$ mixtures, H atoms quickly attach Si dangling bonds and thereby resulted in the formation of Si–H termination. Correspondingly, the scanned regions presented lower Si–H bond densities (see Fig. 9c, d). Subsequent nucleophilic attacks of reactive species on Si–H bonds and polarization of Si–Si backbonds would be the rate-

Figure 9 a–b Schematic diagrams showing the scanning-induced deformation process along the sliding direction. **c–d** Dissolution process of a cross-section of the scanned region in HF/HNO$_3$ mixtures.
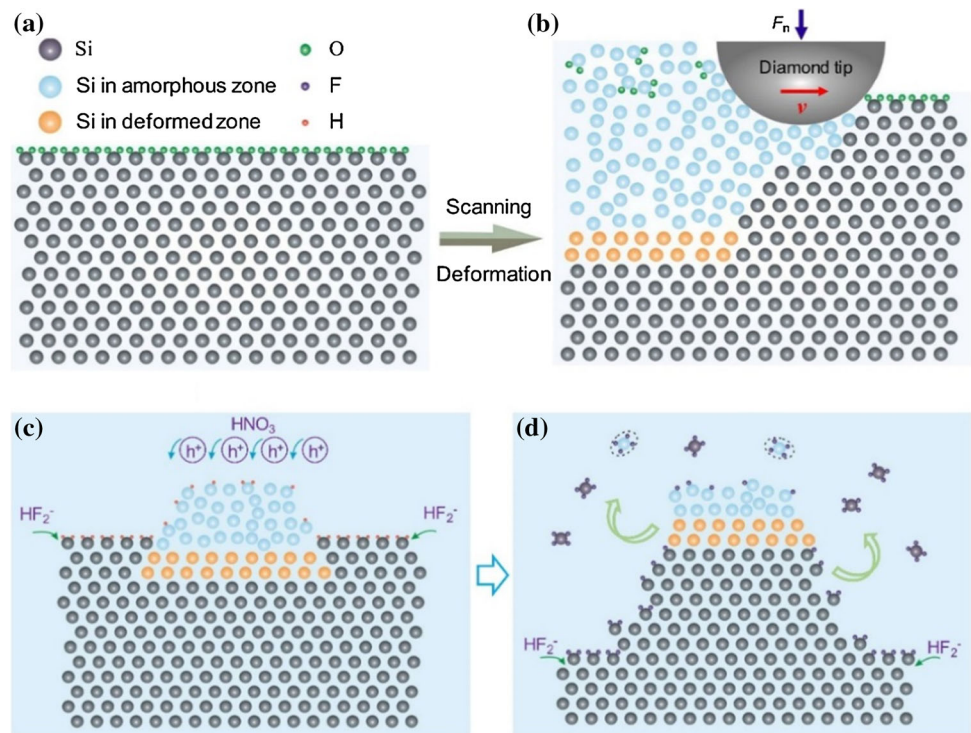
limiting steps, retarding the break out of Si–H bonds and Si–Si backbonds. This, in turn, slowed down the dissolution rate of Si atoms in the scanned regions, resulting in rapid increment of the height of hillock nanostructures on Si surface.

## Fabrication of nondestructive nanostructures on Si surface

By controlling tip scanning traces under close-loop AFM mode, various nondestructive nanostructures can be realized on Si surface through subsequent anisotropic etching in HF/HNO$_3$ mixtures. An array of Si nanogratings with a period of 1.3 μm and a height of ∼ 80 nm is illustrated in Fig. 10a. This array was fabricated at F_n = 40 μN in a line-scanning mode followed by post-etching for 2 s, and the height of asperities is less than ∼ 5 nm. In Fig. 10b, a pentagram structure with a height of ∼ 95 nm was observed. This structure was fabricated at F_n = 40 μN followed by post-etching for 2 s. In Fig. 10c, a spiral line structure with a height of ∼ 90 nm was produced at F_n = 40 μN followed by post-etching for 2 s. Also, by designing the layout of friction-induced hillocks, a note structure with a height of ∼ 90 nm was formed at F_n = 40 μN followed by post-etching for 2 s (Fig. 10d).

In sum, the proposed approach possessed an excellent ability for rapid fabrication of nondestructive nanostructures. Also, it did not require additional fields or templates. In traditional SPM-based direct writing technology, a sharp diamond tip would be applied to produce groove-shaped scratch under high contact pressure at the interface between the tip and sample. Although direct scratching is characterized by high precision, it could be unstable due to probe wear during the scratching process. By contrast, the P_{max} of ∼ 2.1–9.8 GPa used during the preparation process of friction-induced hillocks was less than critical contact pressure (P_y) of initial yield of Si, which can be estimated as ∼ 11.3 GPa by Eq. (1):

$$P_y = \frac{1}{0.31(\tau_c)_{max}} \leq 1.61\delta_y \tag{1}$$

Note that Eq. (1) was derived from the relationship between principal shear stress (τ_c) and P_{max} (τ_c = 0.31 P_{max}), and Tresca yield criterion (τ_c)$_{max} \leq 0.5$ δ_y. Here, yield stress (δ_y) of monocrystalline Si was ∼ 7 GPa. Therefore, friction-induced hillocks were produced before yield failure of Si material. Moreover, the scanning method could extend the lifetime of the probe due to the relatively low contact pressure.

Figure 10 A series of nondestructive Si nanostructures fabricated by the proposed approach: **a** nanogratings array, **b** a pentagram, **c** spiral line, and **d** a note.
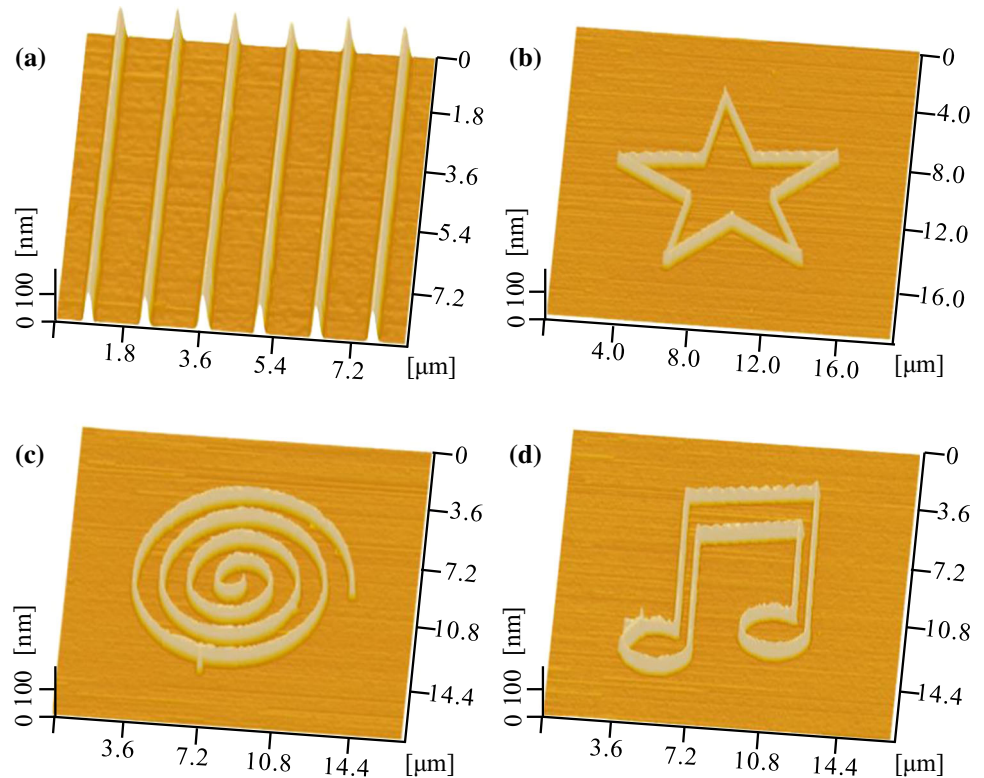
On the other hand, anisotropic etchants were widely applied in Si bulk micromachining, while HF/HNO₃ mixtures were considerable to be difficult in nanostructuring of Si substrates due to the absence of no preference for particular crystal planes. Fortunately, the friction-induced hillocks exhibited strong anti-etching abilities in HF/HNO₃ mixtures, resulting in the formation of hillock nanostructures on Si surface. Moreover, diverse cross-sectional contours of fabricated hillock structures were flexibly realized, which can hardly be produced by anisotropic etchants etching due to their intrinsic etching selectivity. Furthermore, the fabricated hillock structures were defect-free, thereby potentially applying in the patterning of Si substrates for the growth of high-quality epitaxial layers. Also, further design and optimization of scanning tracks may prepare high-quality optical structures, such as diffraction gratings and circular gratings for use in photodetectors [35]. Hence, the proposed approach may open a new SPM-based nanofabrication paradigm when considering the above advantages and potential application value.

Conclusions

Fast and anisotropic etching method was successfully developed for the fabrication of high-quality nanostructures on Si surfaces to overcome the limitation of isotropic etching of Si in HF/HNO₃ mixtures. Several affecting parameters were evaluated and the results were analyzed. The proposed method looks very promising for the fabrication of controllable nano-sized functional Si-based devices by HF/HNO₃ mixtures. The following conclusions can be drawn:

(1) The distinctive anisotropic etching in HF/HNO₃ mixtures was significantly dependent on volume ratio, sliding cycle, normal load, and etching time. The mixtures with volume ratios from 1:100 to 1:5 presented excellent anisotropic etching abilities for the fabrication of hillock nanostructures with different cross-sectional profiles. As volume ratio rose, the fabrication height first gradually increased and then decreased, and the maximum height was observed at ratio 1:60 while the fabrication width remained stable. Comprehensive consideration of fabrication results and efficiency determined the most suitable sliding cycle

N for anisotropic etching of scanned regions as 100. The fabrication height/width can be effectively controlled by normal load and etching time.

(2) AFM topographies of a friction-induced hillock before and after being etched by HF and HF/HNO$_3$ mixtures revealed that a-Si can resist HF/HNO$_3$ mixtures etching, while deformed Si provided little contribution for rapid generation of hillock nanostructures. Moreover, HRTEM images displayed defect-free nanostructures.

(3) Further analysis based on an electrochemical dissolution model suggested that lower average dangling bond density in scanned regions can retard the breakup of Si–H bonds and polarized Si–Si backbonds, leading to lower dissolution rates of Si atoms in the scanned regions.

Acknowledgements

Compliance with ethical standards

Conflict of interest The authors declare that they have no conflict of interest.

Electronic supplementary material: The online version of this article (https://doi.org/10.1007/s10853-020-05452-2) contains supplementary material, which is available to authorized users.

References

[1] Li YM, Somorjai GA (2010) Nanoscale advances in catalysis and energy applications. Nano Lett 10:2289–2295

[2] Tripp RA, Dluhy RA, Zhao YP (2008) Novel nanostructures for SERS biosensing. Nano Today 3:31–37

[3] Hong AJ, Liu CC, Wang Y, Kim J, Xiu FX, Ji SX, Zou J, Nealey PF, Wang KL (2010) Metal nanodot memory by self-assembled block copolymer lift-off. Nano Lett 10:224–229

[4] Priolo F, Gregorkiewicz T, Galli M, Krauss TF (2014) Silicon nanostructures for photonics and photovoltaics. Nat nanotechnol 9:19–32

[5] Achal R, Rashidi M, Croshaw J, Churchill D, Taucer M, Huff T, Cloutier M, Pitters J, Wolkow RA (2018) Lithography for robust and editable atomic-scale silicon devices and memories. Nat Commun 9:2778

[6] Nayak BK, Iyengar VV, Gupta MC (2011) Efficient light trapping in silicon solar cells by ultrafast-laser-induced self-assembled micro/nano structures. Prog Photovoltaics 19:631–639

[7] Duan XF, Zhou GR, Huang YQ, Shang YF, Ren XM (2015) Theoretical analysis and design guideline for focusing sub-wavelength gratings. Opt express 23:2639–2646

[8] Tang QT, Shen HL, Yao HY, Gao K, Ge JW, Liu YW (2020) Investigation of optical and mechanical performance of inverted pyramid based ultrathin flexible c-Si solar cell for potential application on curved surface. Appl Surf Sci 504:144588

[9] Liu JL, Zhang JL, Mao QH, Wu XM, Jiang FY (2013) Effects of AlN interlayer on growth of GaN-based LED on patterned silicon substrate. CrystEngComm 15:3372–3376

[10] Regonda S, Tian RH, Gao JM, Greene S, Ding JH, Hu W (2013) Silicon multi-nanochannel FETs to improve device uniformity/stability and femtomolar detection of insulin in serum. Biosens Bioelectron 45:245–251

[11] Wu YQ, Huang H, Zou J, Dell JM (2009) Nanoscratch-induced deformation of single crystal silicon. J Vac Sci Technol B 27:1374–1377

[12] Wu L, Yu BJ, Fan ZT, Zhang P, Feng CQ, Chen P, Ji JX, Qian LM (2020) Effects of normal load and etching time on current evolution of scratched GaAs surface during selective etching. Mater Sci Semicon Proc 105:104744

[13] Guo GR, Li JM, Deng CB, He QP, Yu QY, Zhou C, Liu XX, Jiang SL, Chen L, Yu BJ, Qian LM (2018) Nondestructive nanofabrication on monocrystalline silicon via site-controlled formation and removal of oxide mask. Appl Phys Express 11:116501

[14] Guo J, Yu BJ, Chen L, Qian LM (2015) Nondestructive nanofabrication on Si (100) surface by tribochemistry-induced selective etching. Sci Rep 5:16472

[15] Chou SY, Keimel C, Gu J (2002) Ultrafast and direct imprint of nanostructures in silicon. Nature 417:835–837

[16] Sievilä P, Chekurov N, Tittonen I (2010) The fabrication of silicon nanostructures by focused-ion-beam implantation and TMAH wet etching. Nanotechnology 21:145301

[17] Ryu Cho YK, Rawlings CD, Wolf H, Spieser M, Bisig S, Reidt S, Sousa M, Khanal SR, Jacobs TDB, Knoll AW (2017) Sub-10 nanometer feature size in silicon using thermal scanning probe lithography. ACS Nano 11:11890–11897

[18] Meng BB, Yuan DD, Zheng J, Qiu P, Xu SL (2020) Tip-based nanomanufacturing process of single crystal SiC:

ductile deformation mechanism and process optimization. Appl Surf Sci 500:144039

[19] Guo J, Song CF, Li XY, Yu BJ, Dong HS, Qian LM, Zhou ZR (2012) Fabrication mechanism of friction-induced selective etching on Si (100) surface. Nanoscale Res Lett 7:152

[20] Wu L, Fan ZT, Peng Y, Zhou HC, Wang HB, Yu BJ, Qian LM (2019) Rapid nanofabrication via UV-assisted selective etching on GaAs without templates. Chem Phys Lett 717:152–157

[21] Song CF, Li XY, Cui SX, Dong HS, Yu BJ, Qian LM (2013) Maskless and low-destructive nanofabrication on quartz by friction-induced selective etching. Nanoscale Res Lett 8:140

[22] Zhou C, Li JM, Wu L, Guo GR, Wang HB, Chen P, Yu BJ, Qian LM (2018) Friction-induced selective etching on silicon by TMAH solution. RSC Adv 8:36043–36048

[23] Rietig A, Langner T, Acker J (2019) A revised model of silicon oxidation during the dissolution of silicon in HF/HNO3 mixtures. Phys Chem Chem Phys 21:22002–22013

[24] Acker J, Langner T, Meinel B, Sieber T (2018) Saw damage as an etch mask for the acidic texturization of multicrystalline silicon wafers. Mater Sci Semicon Proc 74:238–248

[25] Chen CY, Wong CP (2015) Unveiling the shape-diversified silicon nanowires made by HF/HNO$_3$ isotropic etching with the assistance of silver. Nanoscale 7:1216–1223

[26] Steinert M, Acker J, Oswald S, Wetzig K (2007) Study on the mechanism of silicon etching in HNO3-rich HF/HNO$_3$ mixtures. J Phys Chemi C 111:2133–2140

[27] Wu L, Yu BJ, Zhang P, Feng CQ, Chen P, Deng L, Gao J, Chen SM, Jiang SL, Qian LM (2020) Rapid identification of

ultrathin amorphous damage on monocrystalline silicon surface. Phys Chem Chem Phys 22:12987–12995

[28] Wang HB, Deng CB, Xiao C, Liu LY, Liu JW, Peng Y, Yu BJ, Qian LM (2019) Fast and maskless nanofabrication for high-quality nanochannels. Sens Actuat B-Chem 288:383–391

[29] Mir A, Luo XC, Sun JN (2016) The investigation of influence of tool wear on ductile to brittle transition in single point diamond turning of silicon. Wear 364–365:233–243

[30] Yu BJ, Li XY, Dong HS, Chen YF, Qian LM, Zhou ZR (2012) Towards a deeper understanding of the formation of friction-induced hillocks on monocrystalline silicon. J Phys D Appl Phys 45:145301

[31] Johnson KL (1985) Contact mechanics. Cambridge University Press, Cambridge, UK

[32] Minor AM, Lilleodden ET, Jin M, Stach EA, Chrzan DC, Morris JW (2005) Room temperature dislocation plasticity in silicon. Philos Mag 85:323–330

[33] Turner DR (1960) On the mechanism of chemically etching germanium and silicon. J Electrochem Soc 107:810

[34] Biegelsen DK, Stutzmann M (1986) Hyperfine studies of dangling bonds in amorphous silicon. Phys Rev B 33:3006–3011

[35] Duan XF, Wang JC, Huang YQ, Liu K, Shang YF, Zhou GR, Ren XM (2016) Mushroom-mesa photodetectors using subwavelength gratings as focusing reflectors. IEEE Photonic Tech Lett 28:2273–2276